SI Appendix

Yangjin Kim[a,b], Ji Young Yoo[c], Tae Jin Lee[c], Joseph Liu[e], Jianhua Yu[f], Michael A Caligiuri[g], Balveen Kaur[c], and Avner Friedman[a,d,1]

[a]Mathematical Biosciences Institute, Ohio State University, Columbus, OH, 43210, USA; [b]Department of Mathematics, Konkuk University, Seoul, 143-701, Republic of Korea; [c]Department of Neurosurgery, University of Texas Health Science Center at Houston, TX 77030, USA; [d]Department of Mathematics, Ohio State University, Columbus, OH, 43210, USA; [e]Department of Neurological Surgery, The Ohio State University Wexner Medical Center, Columbus, OH, 43210, USA; [f]Division of Hematology, Department of Internal Medicine, The Ohio State University Wexner Medical Center, Columbus, OH, 43210, USA; [g]City of Hope National Medical Center, Duarte, CA. 91010, USA

[1]To whom correspondence should be addressed. E-mail: afriedman@math.osu.edu, Balveen.Kaur@uth.tmc.edu

Mathematical Model Development

Boundary and Initial Conditions

Boundary Condition:
We take no-flux boundary condition for all variables (x, y, n, K, K', v, B) at the origin and

$$\frac{dX}{dt} = \boldsymbol{u}, \text{ on } \Gamma(t) \tag{1}$$

$$\frac{\partial v}{\partial \nu} = 0, \text{ on } \partial\Omega_0, \tag{2}$$

where ν is the outer normal vector and $X = X(t)$ represents the free boundary.

Initial Condition:
The initial conditions are given as follows:

$$x(r,0) = 0.49 * (1.0 + \tanh(-(r - 0.09)/0.01)) \tag{3}$$

$$y(r,0) = 0.0 \tag{4}$$

$$n(r,0) = 0.0 \tag{5}$$

$$K(r,0) = 0.01 * (1.0 + \tanh(-(r - 0.09)/0.01)) \tag{6}$$

$$K'(r,0) = 0.0 \tag{7}$$

$$v(r,0) = 1.0 \tag{8}$$

$$B(r,0) = 0.0 \tag{9}$$

Nondimensionalization

In the simulations of the model we used the non-dimensionalization described below, but we presented the final results in dimensional form.

Variable	Description	Dimensional value	Ref
L	Length scale	3 mm	[11]
T	Time scale	1 h	
Θ	Typical cell density	10^6 $cells/mm^3$	[2, 9]
v^*	virus concentration	2.2×10^8 $virus/mm^3$	[2, 9]
B^*	Bortezomib concentration	1.0×10^{-11} g/mm^3	[11, 12]

Table S1. Reference value used in the mathematical model.

Nondimensionalized Variables and Parameters.

$$\begin{aligned}
&\bar{t} = \frac{t}{T},\ \bar{x} = \frac{x}{\Theta},\ \bar{y} = \frac{y}{\Theta},\ \bar{n} = \frac{n}{\Theta},\ \bar{v} = \frac{v}{v^*},\ \bar{K} = \frac{K}{\Theta},\ \bar{K'} = \frac{K'}{\Theta},\ \bar{D} = \frac{D}{\tilde{D}},\ \bar{D}_v = \frac{D_v}{\tilde{D}},\ \bar{D}_B = \frac{D_B}{\tilde{D}},\\
&\bar{\lambda} = T\lambda,\ \bar{x}_0 = \frac{x_0}{\Theta},\ \bar{\beta} = Tv^*\beta,\ \bar{\beta}_1 = TB^*\beta_1,\ \bar{\gamma_1} = T\Theta\gamma_1,\ \bar{\gamma_1'} = T\Theta\gamma_1',\ \bar{\delta} = T\delta,\ \bar{\beta}_2 = TB^*\beta_2\\
&\bar{\gamma_2} = T\Theta\gamma_2,\ \bar{\gamma_2'} = T\Theta\gamma_2',\ \bar{\mu} = T\mu,\ \bar{b} = \frac{b\Theta}{v^*},\ \bar{\gamma} = T\gamma,\ \bar{\alpha}_1 = B^*\alpha_1,\ \bar{I}_B = \frac{TI_B}{B^*},\ \bar{k}_B = \frac{k_B}{B^*},\\
&\bar{\mu}_1 = \frac{T\Theta\mu_1}{B^*},\ \bar{\mu}_2 = \frac{T\Theta\mu_2}{B^*},\ \bar{\mu}_B = T\mu_B,\ \bar{\lambda}_1 = T\lambda_1,\ \bar{\alpha}_2 = \alpha_2,\ \bar{\mu}_K = T\mu_K,\ \bar{\lambda}_{NK} = \frac{T\lambda_{NK}}{\Theta},\\
&\bar{\mu}_{K'} = T\mu_{K'}.
\end{aligned} \tag{10}$$

Dimensionless Model Equations.

$$\frac{\partial \bar{x}}{\partial \bar{t}} + \bar{\nabla}\cdot(\bar{x}\bar{\boldsymbol{u}}) = \bar{\nabla}\cdot(\bar{D}\bar{\nabla}\bar{x}) + \bar{\lambda}\bar{x}(1-\bar{x}/\bar{x}_0) - \bar{\beta}\bar{x}\bar{v} - \bar{\beta}_1\bar{x}\bar{B} - \bar{\gamma_1}\bar{x}\bar{K} - \bar{\gamma_1'}\bar{x}\bar{K'}, \tag{11}$$

$$\frac{\partial \bar{y}}{\partial \bar{t}} + \bar{\nabla}\cdot(\bar{y}\bar{\boldsymbol{u}}) = \bar{\nabla}\cdot(\bar{D}\bar{\nabla}\bar{y}) + \bar{\beta}\bar{x}\bar{v} - \bar{\delta}\bar{y} - \bar{\beta}_2\bar{y}\bar{B} - \bar{\gamma_2}\bar{y}\bar{K} - \bar{\gamma_2'}\bar{y}\bar{K'}, \tag{12}$$

$$\frac{\partial \bar{n}}{\partial \bar{t}} + \bar{\nabla}\cdot(\bar{n}\bar{\boldsymbol{u}}) = \bar{\nabla}\cdot(\bar{D}\bar{\nabla}\bar{n}) + \bar{\delta}\bar{y} + \bar{\beta}_2\bar{y}\bar{B} - \bar{\mu}\bar{n}, \tag{13}$$

$$\frac{\partial \bar{K}}{\partial \bar{t}} + \bar{\nabla}\cdot(\bar{K}\bar{\boldsymbol{u}}) = \bar{\nabla}\cdot(\bar{D}\bar{\nabla}\bar{K}) + \bar{\lambda_1}\bar{n}\left(1 + \bar{\alpha_2}\frac{\bar{B}}{\bar{k}_B + \bar{B}}\right) - \bar{\mu}_K\bar{K}, \tag{14}$$

$$\frac{\partial \bar{K'}}{\partial \bar{t}} + \bar{\nabla}\cdot(\bar{K'}\bar{\boldsymbol{u}}) = \bar{\nabla}\cdot(\bar{D}\bar{\nabla}\bar{K'}) + \bar{\lambda}_{NK}I_{[\bar{t}_1,\bar{t}_1+\bar{\tau}]} - \bar{\mu}_{K'}\bar{K'}, \tag{15}$$

$$\frac{\partial \bar{v}}{\partial \bar{t}} = \bar{\nabla}\cdot(\bar{D}_v\bar{\nabla}\bar{v}) + \bar{b}\bar{\delta}\bar{y}(1 + \bar{\alpha}_1\bar{B}) - \bar{\gamma}\bar{v}, \tag{16}$$

$$\frac{\partial \bar{B}}{\partial \bar{t}} = \bar{\nabla}\cdot(\bar{D}_B\bar{\nabla}\bar{B}) + \bar{I}_B - (\bar{\mu_1}\bar{x} + \bar{\mu_2}\bar{y})\frac{\bar{B}}{\bar{k}_B + \bar{B}} - \bar{\mu}_B\bar{B}, \tag{17}$$

$$\begin{aligned}
\bar{\nabla}\cdot\bar{u} = {}& \bar{\lambda}\bar{x}(1-\bar{x}/\bar{x}_0) - \bar{\beta}_1\bar{x}\bar{B} - \bar{\gamma_1}\bar{x}\bar{K} - \bar{\gamma_1'}\bar{x}\bar{K'} - \bar{\gamma_2}\bar{y}\bar{K} - \bar{\gamma_2'}\bar{y}\bar{K'} - \bar{\mu}\bar{n}\\
&+\bar{\lambda_1}\bar{n}\left(1 + \bar{\alpha}_2\frac{\bar{B}}{\bar{k}_B + \bar{B}}\right) - \bar{\mu}_K\bar{K} + \bar{\lambda}_{NK}I_{[\bar{t}_1,\bar{t}_1+\bar{\tau}]} - \bar{\mu}_{K'}\bar{K'}
\end{aligned} \tag{18}$$

Parameter estimation

Diffusion coefficient of cells D is 3.6×10^{-6} mm^2/h. From the approximation $D_v \sim 10^4 D$ [3], we get $D_v = 3.89 \times 10^{-2}$ mm^2/h.

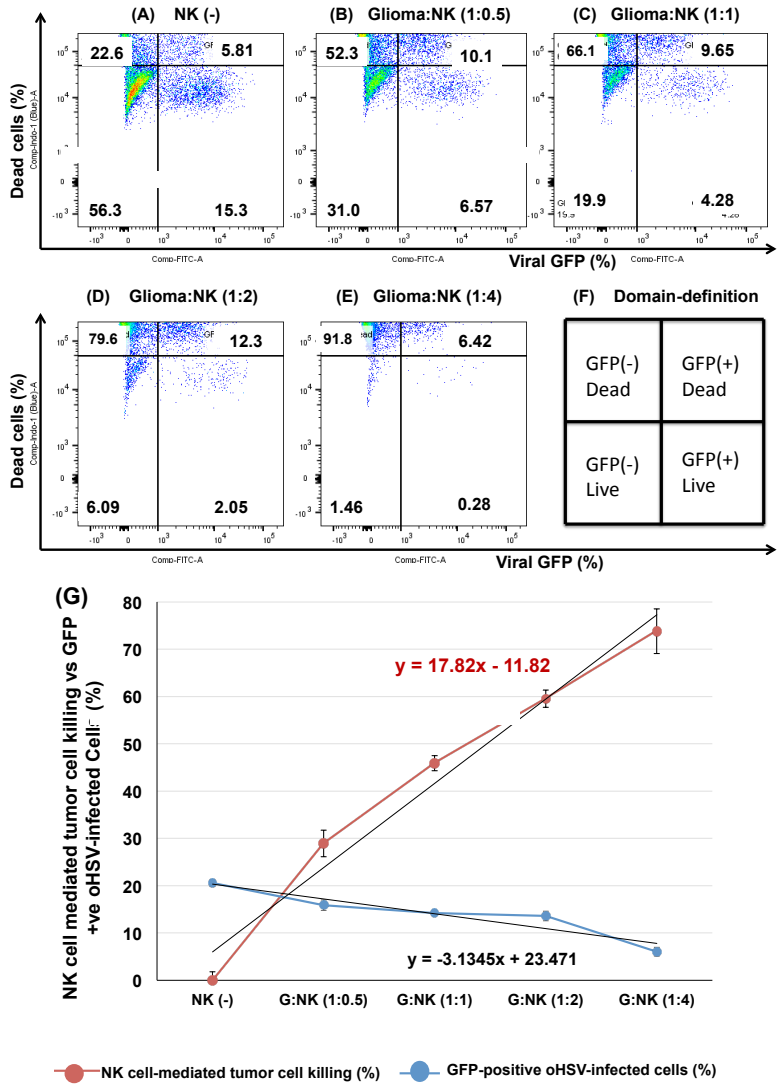

Figure S1. Adjuvant NK cell treatment significantly enhances bortezomib and oHSV-treated glioma cell killing as dose dependent manner. U251T3-mCherry cells which stably express mCherry, were pretreated with or without bortezomib for 16 hours followed by oHSV treatment at an MOI of 0.01 (ED50). Two hours post oHSV infection, cells were washed to remove unbound virus and then overlaid with different number of primary donor-derived human NK cells. Twenty-four hours later, cells were harvested and stained with a Live/Dead Fixable Aqua Dead Cell staining solution. (A-E) Representative scatter plots for various glioma:NK ratios: NK(-) (A), 1:0.5 (B), 1:1 (C), 1:2 (D), 1:4 (E). (F) Definition of areas in each subpanel in (A-E) based on GFP(+/-) status and live/dead status. (G) NK cell mediated tumor cell killing versus GFP-positive oHSV-infected tumor cells (%) for various glioma:NK ratios in (A-E). Errors bars represent ±SD for each group.

Cell killing rates $(\beta_1, \beta_2, \gamma_1, \gamma_2, \gamma_1', \gamma_2')$: We assume that the effect of $B-necroptosis$ of y is larger than $B-apoptosis$ for x as indicated in previous studies [11,12], and NK cells kill more effectively y cells, and take $\beta_2 = 2\beta_1, \quad \gamma_2 = 10\gamma_1$. We assume that K' is more efficient than K in killing cancer cells, and take

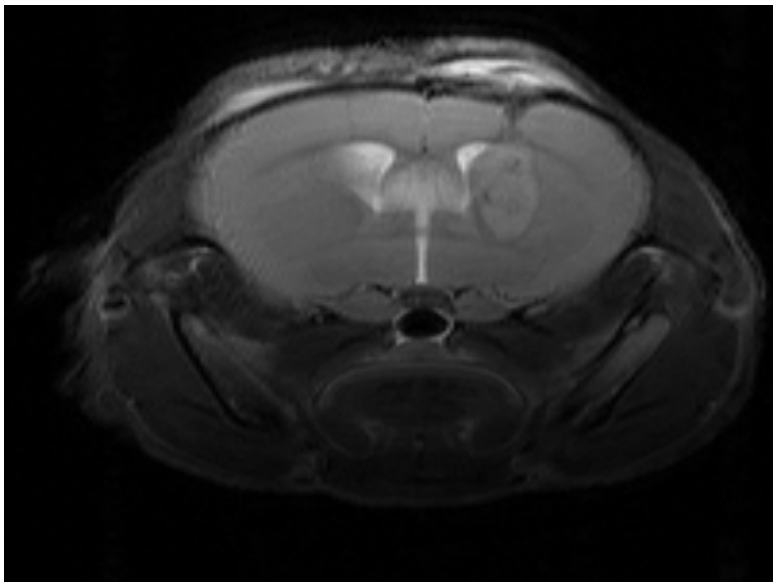

Figure S2. Mice were implanted intracranially with patient derived primary GBM (GBM30) cells and treated with oHSV 10 days post tumor implantation. Tumor-bearing half-hemispheresharvested 3 days after the viral treatments were subjected to NK cell counting by Flow cytometry. Approximately 2,000 NK cells were infiltrated into the oHSV-treated tumor-bearing brain hemisphere compared to approximately 360 NK cells found to be infiltrated into the PBS-treated control brain hemisphere. Dynamic contrast enhanced MRI (DCE-MRI) showed representative images of coronal brain sections of intracranial glioma-bearing mice 10 days post tumor implantation. Implantation of 1×10^5 tumor cells has caused an approximately 3.35 mm^3 size of tumor after 13 days. Based on these observations, the ratio of NK cells to tumor cells is likely much lower than 1:10.

$\gamma_1' = 3\theta\gamma_1,\ \gamma_2' = 3\theta\gamma_2$ where $0 < \theta < 1$.

α_1: We assume that B doubles when the replication of v when $B = B^*$, $1 + \alpha_1 B^* = 2$ [12], leading to $\alpha_1 = 10^{11}\ mm^3/g$.

k_B: We take the reference value of bortezomib to indicate the instant consumption of bortezomib by uninfected and infected tumor cells, and activation of endogenous NK cells, leading to $k_B = B^* = 1.0 \times 10^{-11}\ g/mm^3$.

μ_B: The average half-life of Bortezomib is 10-31 hours [6]. The mean elimination half-life of after the 1st dose was in a range of 9-15 hours at dose level 1.45-2.00 mg/m^2 in patients [4]. We take 20 h, leading to $\mu_B = \frac{ln2}{20\ h} = 3.47 \times 10^{-2}/h$.

μ_1, μ_2: Bortezomib has a long half-life of 31 hours while internalization of bortezomib into an infected cell and infection of tumor cells happen at a much faster time scale. Therefore, we assume that the consumption term in equation (17) is much bigger than natural decay term, leading to $(\mu_1 x + \mu_2 y)\frac{1}{2} > 0.166B > \mu_B B$ with an estimation of $\frac{B}{k_1+B} \sim 0.5$. By setting $\mu_1 = \mu_2$ and an estimation of $x+y \sim 0.8\times10^{-3}\ g/mm^3$, we get $\mu_1 = \mu_2 = \frac{0.166\times10^{-8}}{0.8}\frac{1}{h} = 2.075 \times 10^{-9}/h$.

α_2: Endogenous NK cells are activated by the presence of necrotic cells at the rate of λ_1. We assume that recruitment of endogenous NK cells (K) by necrotic cells will be doubled in the presence of bortezomib.

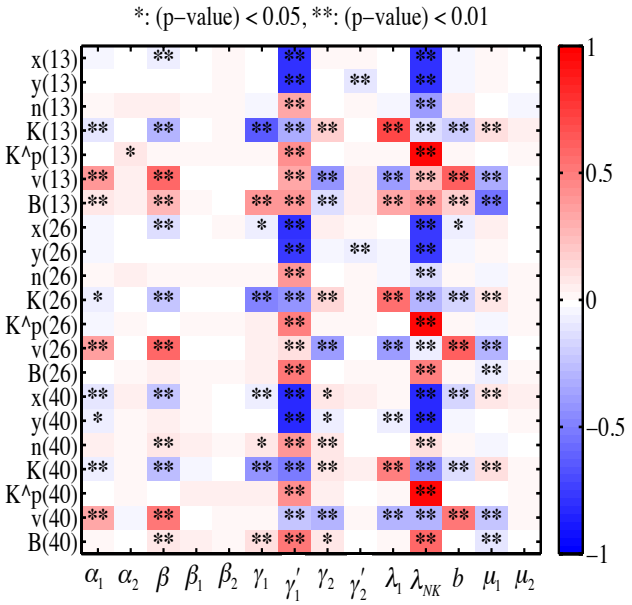

Figure S3. Sensitivity Analysis using General Latin Hypercube Sampling (LHS) scheme and Partial Rank Correlation Coefficient (PRCC) was performed on the current model. The reference output in color is PRCC values (red for positive PRCC values; blue for negative PRCC values) for the populations of uninfected cancer cells ($\hat{x}(t) = \int_{\Omega(t)} x(r,t)\ dr$), infected cancer cells ($\hat{y}(t) = \int_{\Omega(t)} y(r,t)\ dr$), necrotic cancer cells ($\hat{n}(t) = \int_{\Omega(t)} n(r,t)\ dr$), endogenous NK cells ($\hat{K}(t) = \int_{\Omega(t)} K(r,t)\ dr$), exogenous NK cells ($\hat{K'}(t) = \int_{\Omega(t)} K'(r,t)\ dr$), and oncolytic viruses ($\hat{v}(t) = \int_{\Omega(t)} v(r,t)\ dr$), and bortezomib level ($\hat{B}(t) = \int_{\Omega(t)} B(r,t)\ dr$) at time $t = 13, 26, 40\ days$.

We assume that B doubles the proliferation of K when $B = B^*$. We also assume that in steady state, $\frac{B}{k_B+B} \sim \frac{1}{2}$. Hence, $1 + \alpha_2 \frac{1}{2} = 2$, leading to $\alpha_2 = 2.0$.

$\mu_K, \mu_{K'}$: In young and healthy individuals, the average half-life of NK cells was estimated to be 10 days [13]. The half-life of mature NK cells was measured to be 7-8 days [1,5,10]. We take the half-life of NK cells 7 days. Since $ln(2)/(7days) = 0.099/day \sim 0.1/day$, we take $\mu_K = 0.1/day = 4.1 \times 10^{-3}\ h^{-1}$. We also assume that $\mu_{K'} = \mu_K = 4.1 \times 10^{-3}\ h^{-1}$.

The list of parameters and their values are given in Tables S2,S1.

Sensitivity Analysis

The model contains 27 parameters, many of whom are available in the literature or can be estimated, but there are some for which no experimental data are known or which are important to carefully determine. These parameters are $\alpha_1, \alpha_2, \beta, \beta_1, \beta_2, \gamma_1, \gamma_1', \gamma_2, \gamma_2', \lambda_1, \lambda_{NK}, b, \mu_1, \mu_2$. In order to determine how sensitive is the population of cells and viruses, and bortezomib level after 13, 26 or 40 days to these parameters, we have performed a sensitivity analysis using a method developed in [7] and modifying Matlab files available from the website of Denise Kirschner's Lab: http://malthus.micro.med.umich.edu/lab/usadata/.

We have chosen a physiologically reasonable range for each of these parameters, and divided each range into 1,000 intervals of uniform length, with all other parameters fixed at values given in Ta-

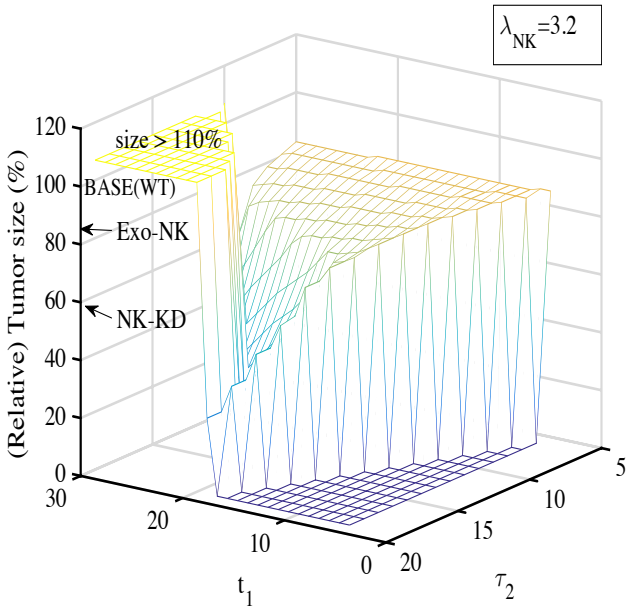

Figure S4. Effect of a new combination therapy (NK cell depletion + NK cell injection) on the relative tumor size in a $t_1 - \tau_2$ plane. Initially, the NK cells were depleted for τ_2 days and NK cells were injected at t_1 days ($t_1 \geq \tau_2$). Parameter: $\lambda_{NK} = 3.2$.

ble S2. For each of the fourteen parameters of interest, a partial rank correlation coefficient (PRCC) value is calculated. The PRCC values range between -1 and 1 with the sign determining whether an increase in the parameter value will decrease (-) or increase (+) the variable of interest at a given time. Both the PRCC values and the associated p-value for the fourteen perturbed parameters are computed and recorded in Fig. S3, which shows the sensitivities to parametric variations for populations of uninfected cancer cells: ($\hat{x}(t) = \int_{\Omega(t)} x(r,t)\ dr$), infected cancer cells: ($\hat{y}(t) = \int_{\Omega(t)} y(r,t)\ dr$), necrotic cancer cells: ($\hat{n}(t) = \int_{\Omega(t)} n(r,t)\ dr$), endogenous NK cells: ($\hat{K}(t) = \int_{\Omega(t)} K(r,t)\ dr$), exogenous NK cells: ($\hat{K'}(t) = \int_{\Omega(t)} K'(r,t)\ dr$), and oncolytic viruses: ($\hat{v}(t) = \int_{\Omega(t)} v(r,t)\ dr$), and concentrations of bortezomib: ($\hat{B}(t) = \int_{\Omega(t)} B(r,t)\ dr$) at t =13, 26, and 40 days. We conclude that (i) the uninfected cancer population is negatively correlated to the parameters $\beta, \gamma_1', \lambda_{NK}, b$, but it is weakly correlated with $\alpha_1, \alpha_2, \beta_1, \beta_2, \gamma_1, \gamma_2, \gamma_2', \lambda_1, \mu_1, \mu_2$. (ii) the infected cancer population is negatively correlated to the parameters γ_1', λ_{NK}, but it is weakly correlated with other parameters ($\beta, b, \alpha_1, \alpha_2, \beta_1, \beta_2, \gamma_1, \gamma_2, \gamma_2', \lambda_1, \mu_1, \mu_2$). (iii) the endogenous NK population is positively correlated to the parameters λ_1, but negatively correlated with $\gamma_1, \gamma_1', \lambda_{NK}$. (iv) the exogenous NK population is positively correlated with γ_1', λ_{NK}, but is weakly correlated with other parameters. (v) OV population is positively correlated to the parameters α_1, β, b, but is negatively correlated to the parameters $\gamma_1, \gamma_2, \lambda_1, \lambda_{NK}, \mu_1$. While high level of sensitivity of OV population to replication rate b is obvious, inhibition sensitivity of OV replication by NK cells through γ_2 can explain why depletion of endogenous NK cells can increase oncolytic tumor cell killing, increasing anti-tumor killing potential (Fig. 5B in the text). (vi) Bortezomib level is positively (or negatively) correlated to the parameters γ_1', λ_{NK} (or μ_1), with little correlation with other parameters. These results are consistent with our findings that external injection or depletion of NK cells (K, K') plays a critical role in bortezomib-assist OV therapy in glioblastoma.

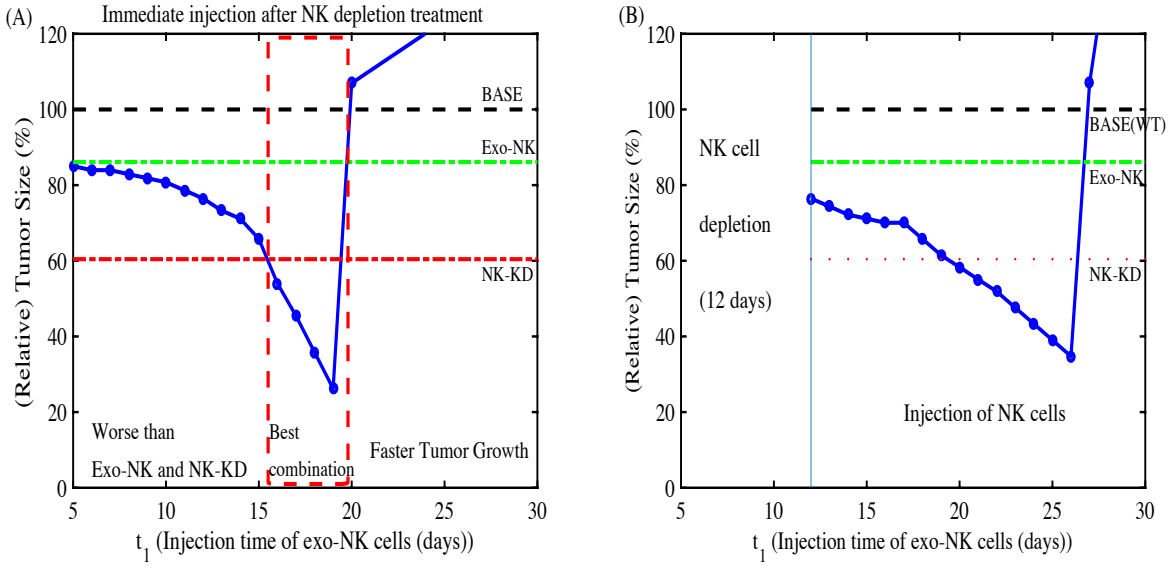

Figure S5. Nonlinear effect of combination therapy (NK cell depletion+exo-NK cell injection) on the tumor size for various injection time $t_1 = 12, 13, \ldots, 30$ *days* of NK cells after initial NK depletion ($\tau_2 = 12$ *days*). (A) The relative tumor size in response to NK cell injection at various injection time points immediately after NK cell depletion. (B) The relative tumor size in response to various injection time points of NK cells after the 12 days of NK cell depletion process ($\tau_2 = 12$ *days* fixed). The tumor sizes in cases of base (WT), NK cell depletion alone (NK-KD), NK cell injection alone (Exo-NK) were marked in dashed (black), dotted (red), and dash-dot (green) lines, respectively. The anti-tumor efficacy of the combination therapy relative to the base therapy depends on the schedule of NK cell injection. Parameter: $\lambda_{NK} = 3.2$.

Development of a new combination therapy: NK cell injection after NK cell depletion

We showed the nonlinear behavior of tumor growth in response to cases either when NK cells were removed from tumor microenvironment (TME) by anti-Asialo-GM1 antibody (NK-KD) or when exogenous NK cells were introduced to the system (Exo-NK). See Fig. 3 and Fig 5A in the main text. It would be interesting to see the effect of a new combination strategy on the tumor size by initially depleting NK cells for the duration of τ_2 days and intratumorally injecting NK cells at time t_1 (Here, we assume $t_1 \geq \tau_2$). Fig. S4 shows the tumor size relative to the base case (100%) at final time in response to various schedules in the $t_1 - \tau_2$ plane. The relative tumor sizes for complete NK cell depletion by anti-Asialo-GM1 antibody and pure NK cell injection were marked by arrows on the z-axis. The tumor shows the nonlinear behaviors in different combinations of NK depletion duration (τ_2) and injection time (t_1). For most of combinations of t_1, τ_2, the tumor size is smaller than the base case (WT) and the efficacy of this combination therapy is improving as τ_2 and t_1 are increased but remain moderate. However, the model predicts that the anti-tumor efficacy will be significantly reduced for higher values of t_1, τ. Fig. S5A shows the relative tumor size at final time ($t = 40$ *days*) in response to the NK cell injection immediately after the NK cell depletion treatment (i.e., $t_1 = \tau_2$). For a relatively early transition from NK cell depletion to NK cell injection ($t_1 < 15$), the tumor size is smaller than in the base case (WT) and Exo-NK case, but is larger than in the NK-KD case. In this case, an early intervention of NK cell depletion by the combination therapy reduces the OV-mediated tumor cell killing and eradicates the chances of NK cell-mediated

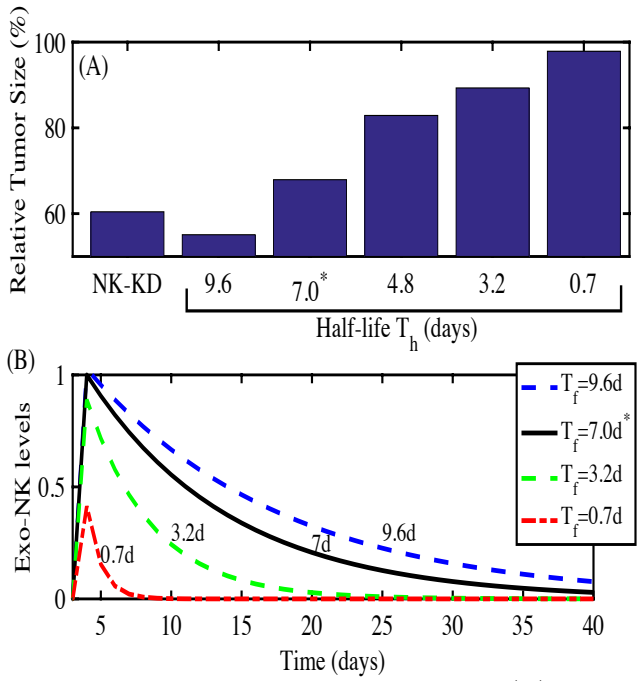

Figure S6. The effect of NK cell retention on anti-tumor efficacy. (A) The relative tumor size in response to NK-KD case and various half-life (T_h) of injected NK cells in tumor microenvironment: $T_h = 9.6, 7.0, 4.8, 3.2, 0.7$ *day*. (B) Time courses of the populations of exogenous NK cells with different half-life: $T_h = 9.6, 7.0, 3.2, 0.7$ *day*. The tumor size was normalized with respect to the base case (WT). $\lambda_{NK} = 5.2$.

control of tumor growth at earlier time points, leading to intermediate anti-tumor efficacy that is lower than one of NK cell depletion (NK-KD). On the other hand, the tumor size is decreased further as the transition time ($t_1 = \tau_2$) is increased. For intermediate transition time points ($15.5 < t_1 < 19.5$), the tumor size is even smaller than in the NK-KD and Exo-NK cases, leading to the best outcome. However, the tumor size jumps to a larger value as the transition time is increased further ($t_1 > 20$), leading to faster tumor growth and lower anti-tumor efficacy. Therefore, the intermediate transition times (red dashed box in the middle) results in the best strategy of reducing the tumor size. Initial depletion of endogenous NK cells in the system upto this optimal transition times enhances tumor cell killing by increased oHSVs and the subsequent NK cell injection further removes the remaining tumor cells from the system, resulting in the best tumor cell killing. When this transition time is significantly delayed, the killing rate of oHSVs in the infected cells by injected NK cells is too big, suppressing OV-mediated tumor cell killing, while the late injection schedule induces low NK cell-mediated tumor cell killing. Therefore, this late timing results in low anti-tumor efficacy. Fig. S5B shows the nonlinear effect of the combination therapy (NK cell depletion followed by NK cell injection) on the tumor size for various injection time points $t_1 = 12, 13, \ldots, 30$ *days* after 12 days of NK cell depletion by anti-Asialo-GM1 antibody treatment. For relatively early time injections ($12 \leq t_1 < 19$ *days*), the combination therapy leads to better than base case and Exo-NK alone. But the anti-tumor efficacy is still lower than in the NK-KD case. However, this tumor size is decreased further as the injection time point (t_1) is further delayed until $t_1 = 26$ *days* ($19 < t_1 < 26$ *days*). For the longer injection time point ($t_1 > 26$ *days*), the tumor size is getting larger because the effect of NK cell depletion is reduced and injection time of new NK cells is too late to control an already large tumor, resulting in the reduced anti-tumor efficacy.

Impact of NK cell retention in tumor microenvironment (TME) on the OV-bortezomib therapy

We investigated the effect of retention time of exogenous NK cells on the final tumor size and the NK cell population in tumor microenvironment. Fig. S6A shows the relative tumor size in response to NK-KD case and various half-life (T_h) of injected NK cells in tumor microenvironment: $T_h = 9.6, 7.0, 4.8, 3.2, 0.7$ *day*. These values correspond to the decay rate of exo-NK cells, $\mu_{K'} = 3.0\times10^{-3}, 4.1\times10^{-3}, 9.0\times10^{-3}, 4.1\times10^{-2}$ h^{-1}, respectively. Fig. S6B shows the time courses of the normalized exogenous NK cell populations for different $\mu_{K'}$'s or $T_h = 9.6, 7.0, 3.2, 0.7$ *day*. The population was normalized relative to the base value in our model, $T_h = 7.0$ *days*. As the half-life decreased, the population of NK cells within the tumor microenvironment decreased (Fig S6B), increasing the tumor size. For example, the population of NK cells in the case of $T_h = 0.7$ *day* quickly disappears from the tumor microenvironment 5 days after the injection (red dashed line in Fig S6B). In our experiments, the exogenous NK cells were introduced by intratumoral injection and the half-life of NK cells is expected to be 7-10 days as other experiments suggested [1, 5, 10, 13]. Therefore, this indicates that the anti-tumor efficacy of the NK cell adjuvant therapy might be poor if the retention rate of exogenous NK cells is lower due to poor indirect transport of NK cells. On the other hand, when the retention capacity of NK cells is higher due to enhanced technology (longer half-life, $T_h = 9.6$ *day*), the tumor size is significantly decreased.

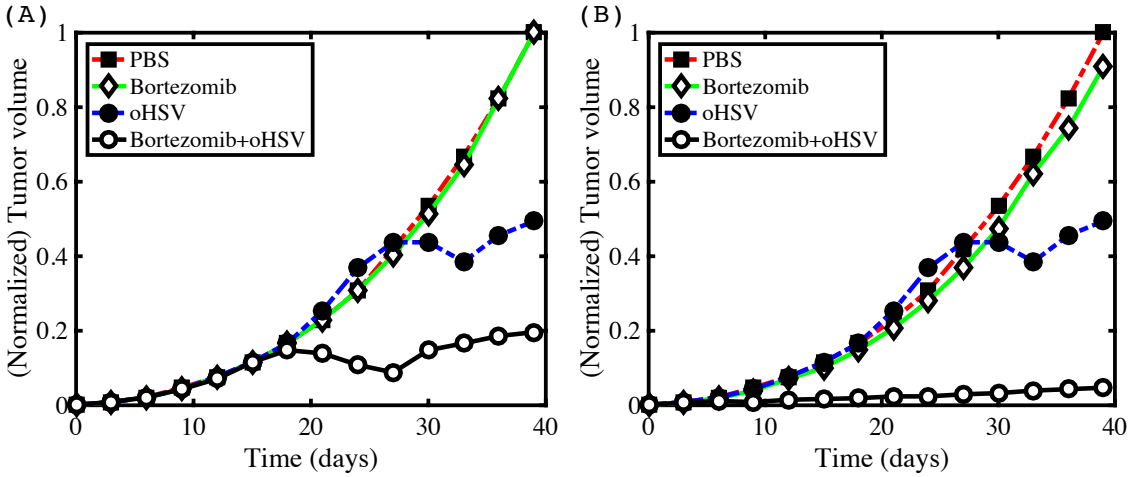

Figure S7. Basic tumor dynamics in the absence of NK cell adjuvant therapy and NK cell depletion. (A) Time courses of tumor volume for wild type (PBS; square), bortezomib treatment (diamond), oHSV treatment (filled circle), and bortezomib+oHSV treatment (empty circle). Parameters: $\beta_1 = 5.0\times10^{-4}$, $\beta_2 = 1.0\times10^{-3}$, $I_B = 1.1\times10^{-1}$. (B) Time courses of tumor volume with enhanced bortezomib sensitivities $\beta_1 = 5.0\times10^{-2}$, $\beta_2 = 5.5\times10^{-1}$, $I_B = 5.5\times10^{-1}$. The tumor volume was normalized with respect to the base case (PBS).

Basic dynamics of the OV-bortezomib treatment without NK cell adjuvant therapy or NK cell depletion

Fig. S7A shows time courses of tumor volume for wild type, bortezomib treatment, oHSV treatment, and bortezomib+oHSV treatment with basic parameter values of bortezomib injection $\beta_1 = 5.0\times10^{-4}$, $\beta_2 = 1.0\times10^{-3}$, $I_B = 1.1\times10^{-1}$. When bortezomib was combined to the oHSV therapy (empty circle), the tumor size was significantly reduced compared to the wild tumor without therapies (PBS, square),

bortezomib alone (diamond), or oHSV alone (filled circle) [11]. The killing rate of a tumor in the presence of bortezomib may depend on cell lines and tumor microenvironment in experiments. For example, mice implanted with GBM169 cells and U251T3 glioma cells show slightly different time curves of tumor growth [11]. But the overall anti-tumor efficacy of bortezomib+oHSV was evident in these cell lines. Fig. S7B shows the time courses of tumor volume for same cases with enhanced bortezomib levels and sensitivities: $\beta_1 = 5.0 \times 10^{-2}$, $\beta_2 = 5.5 \times 10^{-1}$, $I_B = 5.5 \times 10^{-1}$. In this case, the synergetic anti-tumor effect is even further promoted. These results concur well with experimental data [11] and can be used to explore the tumor dynamics in response to NK cell adjuvant therapy and NK cell depletion in this study.

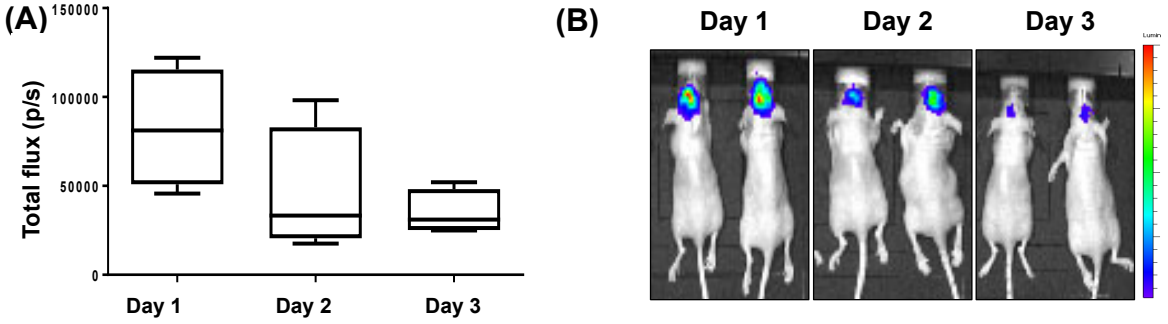

Figure S8. oHSV replication efficacy is reduced in vivo. Nude mice with intracranial patient derived primary GBM30 intracranial tumor were treated with 2×10^5 pfu of an oHSV expressing luciferase (oHSV-Luc). A, data shown are quantification of virally expressed luciferase gene activity in GBM30 intracranial tumors treated with oHSV-Luc on the indicated days. Data shown are total flux in each mouse ($n = 4$). B, representative luciferase images of oHSV-treated mice at the days indicated ($n = 4$).

In vivo luciferase imaging

Nude mice with patient derived primary GBM (GBM30) intracranial tumor were injected intratumorally with 2×10^5 pfu of rHSVQ1-Luc ten days following tumor cell implantation. Mice were imaged on days 1,2, and 3 after oHSV therapy. For in vivo mice luciferase imaging, mice were injected with Luciferin solution (25 mg/ml in PBS, dose of 100 mg/kg, Perkin Elmer, Waltham, MA) by an intraperitoneal injection and anesthetized. The anesthetized mice were placed on non-fluorescent black paper on the imaging platform of an IVIS Lumina II to reduce background noise. Bioluminescence from the anesthetized mice was detected by ZFOV-24 zoom lens-installed IVIS Lumina Series III Pre-clinical In Vivo Imaging System (Perkin Elmer, Waltham, MA). The luminescence intensity was expressed as Averaged Radiance $[p/s/cm^2/sr]$, then normalized by tumor volume (mm^3). See Fig. S8.

References

1. M.A. Cooper, J.E. Bush, T.A. Fehniger, J.B. VanDeusen, R.E. Waite, Y. Liu, H.L. Aguila, and M.A. Caligiuri. In vivo evidence for a dependence on interleukin 15 for survival of natural killer cells. *Blood.*, 100(10):3633–3638, 2002.

2. A. Friedman, J.P. Tian, G. Fulci, E.A. Chiocca, and J. Wang. Glioma virotherapy: effects of innate immune suppression and increased viral replication capacity. *Cancer Res*, 66(4):2314–9, 2006.

3. K. Jacobsen, L. Russell, B. Kaur, and A. Friedman. Effects of CCN1 and macrophage content on glioma virotherapy: A mathematical model. *Bull Math Biol*, 77(6):984–1012, 2015.

4. R.C. Kane, P.F. Bross, A.T. Farrell, and R. Pazdur. The mean elimination half-life of bortezomib after the first dose ranged from 9-15 hours at doses ranging from 1.45?2.00 mg/m2 in patients with advanced malignancies. *The Oncologist*, 8:508–513, 2003.

5. R. Koka, P.R. Burkett, M. Chien, S. Chai, F. Chan, J.P. Lodolce, D.L. Boone, and A. Ma. Interleukin (IL)-15 R[alpha]-deficient natural killer cells survive in normal but not IL-15R[alpha]-deficient mice. *J Exp Med.*, 197(8):977–984, 2003.

6. D. Leveque, M.C.M. Carvalho, and F. MALOISEL. Clinical pharmacokinetics of bortezomib. *In vivo*, 21:273–278, 2007.

7. S. Marino, I. Hogue, C. Ray, and D. Kirschner. A methodology for performing global uncertainty and sensitivity analysis in systems biology. *J Theor Biol*, 254(1):178–96, 2008.

8. W. Mok, T. Stylianopoulos, Y. Boucher, and R.K. Jain. Mathematical modeling of herpes simplex virus distribution in solid tumors: implications for cancer gene therapy. *Clin Cancer Res.*, 15(7):2352–60, 2009.

9. J.A. ODonoghue, M. Bardies, and T.E. Wheldon. Relationships between tumor size and curability for uniformly targeted therapy with beta-emitting radionuclides. *J Nucl Med*, 36(10):1902–9, 1995.

10. K.C. Verbist and K.D. Klonowski. Functions of IL-15 in anti-viral immunity: multiplicity and variety. *Cytokine.*, 59(3):467–478, 2012.

11. J.Y. Yoo, B.S. Hurwitz, C. Bolyard, J. Yu, J. Zhang, K. Selvendiran, K.S. Rath, S. He, Z. Bailey, D. Eaves, T.P. Cripe, D.S. Parris, M.A. Caligiuri, J. Yu, M. Old, and B. Kaur. Bortezomib-induced unfolded protein response increases oncolytic hsv-1 replication resulting in synergistic antitumor effects. *Clin Cancer Res*, 20(14):3787–3798, 2014.

12. J.Y. Yoo, A.C. Jaime-Ramirez, C. Bolyard, H. Dai, T. Nallanagulagari, J. Wojton, B. Hurwitz, T. Relation, J.G. Yu, T. Lee, M.T. Lotze, J. Zhang, C.M. Croce, J. Yu, M.A. Caligiuri, M. Old, and B. Kaur. Bortezomib treatment sensitizes oncolytic hsv-1 treated tumors to nk cell immunotherapy. *Clin Cancer Res*, pii: clincanres.:1003.2016, 2016.

13. Y. Zhang, D.L. Wallace, C.M. de Lara, H. Ghattas, B. Asquith, A. Worth, G. E. Griffin, G.P. Taylor, D.F. Tough, P.C. Beverley, and D. C. Macallan. In vivo kinetics of human natural killer cells: the effects of ageing and acute and chronic viral infection. *Immunology*, 121(2):258–265, 2007.

Parameter	Description	Dimensional value	Source
	Diffusion coefficients/Random motility (mm^2/h)		
D	random motility of cells (x, y, n, K, K')	3.6×10^{-6}	Estimated
D_v	random motility of virus (PBS)	3.89×10^{-2}	[8]
D_B	diffusion coefficient of bortezomib	2.5×10^{-2}	Estimated
	Production/remodeling rates		
λ	proliferation rate of tumor cells	1.8×10^{-1} $1/h$	[2], Estimated
x_0	carrying capacity of uninfected tumor cells	9.98×10^5 $cells/mm^3$	Estimated
β	virus infection rate	1.06×10^{-11} $(mm^3/h\ virus)$	[2]
b	burst size of infected cells	50 $(virus/cell)$	[2]
α_1	bortezomib-induced viral replication rate	10^{11} mm^3/g	Estimated
λ_1	endogenous NK cell activation rate	1.1×10^{-3} h^{-1}	Estimated
α_2	endogenous NK cells activation rate by bortezomib	$2.0^{\dagger}$	Estimated
I_B	bortezomib supply rate	(1.1-5.1)$\times10^{-11}$ $g/(mm^3.h)$	Estimated
	Inhibition/degradation/decay rates		
γ	clearance rate of viruses	1.8×10^{-3} h^{-1}	[2]
δ	infected cell lysis rate	8.2×10^{-2} h^{-1}	[2]
μ	removal rate of dead cells	1.04×10^{-1} h^{-1}	[2]
β_1	bortezomib-induced apoptosis rate	5.0×10^7 $mm^3/(g.h)^{\ddagger}$	Estimated
β_2	bortezomib-induced necroptosis rate	1.0×10^8 $mm^3/(g.h)^{\ddagger}$	Estimated
γ_1	killing rate of uninfected tumor cells by endogenous NK cells	2.9×10^2 $mm^3/(g.h)^{\ddagger}$	Estimated
γ_2	killing rate of infected tumor cells by endogenous NK cells	2.9×10^3 $mm^3/(g.h)^{\ddagger}$ $(\gamma_2 = 10\gamma_1)$	Estimated
γ_1'	killing rate of uninfected tumor cells by exogenous NK cells	$\theta \times 8.7 \times 10^2$ $mm^3/(g.h)^{\ddagger}$ $(\gamma_1' = 3\theta\gamma_1,\ 0 < \theta < 1)$	Estimated
γ_2'	killing rate of infected tumor cells by exogenous NK cells	$\theta \times 8.7 \times 10^3$ $mm^3/(g.h)^{\ddagger}$ $(\gamma_2' = 3\theta\gamma_2,\ 0 < \theta < 1)$	Estimated
μ_1	consumption rate of bortezomib by uninfected tumor cells	2.075×10^{-9} $h^{-1\ddagger}$	Estimated
μ_2	consumption rate of bortezomib by infected tumor cells	2.075×10^{-9} $h^{-1\ddagger}$	Estimated
k_B	Hill-type parameter	1.0×10^{-11} $g/mm^{3\ddagger}$ $(= B^*)$	Estimated
μ_B	decay rate of bortezomib	$3.47 \times 10^{-2}/h$	[4,6]
μ_K	death rate of endogenous NK cells	4.1×10^{-3} h^{-1}	[1,5,10]
$\mu_{K'}$	death rate of exo NK cells	4.1×10^{-3} h^{-1}	[1,5,10]

Table S2. Model parameters. Units are indicated in parenthesis $(\cdot)$ in the third column. †=dimensionless value. $^{\ddagger}1g$ is estimated to be the mass of 10^9 cells.